RSC Advances

PAPER

View Article Online
View Journal | View Issue

Cite this: *RSC Adv.*, 2016, **6**, 45410

Thiophene-*S*,*S*-dioxidized indophenines as high performance n-type organic semiconductors for thin film transistors†

Yunfeng Deng, Bin Sun, Jesse Quinn, Yinghui He, Jackson Ellard, Chang Guo and Yuning Li*

The synthesis of three new isomerically pure (*E*,*E*,*E*)-form thiophene-*S*,*S*-dioxidized indophenine (IDTO) compounds, (3*Z*,3′*Z*)-3,3′-((*E*)-1,1,1′,1′-tetraoxido-5*H*,5′*H*-[2,2′-bithiophenylidene]-5,5′-diylidene)bis(1-dodecyl-indolin-2-one) (**4a-S1**), (3*Z*,3′*Z*)-3,3′-((*E*)-1,1,1′,1′-tetraoxido-5*H*,5′*H*-[2,2′-bithiophenylidene]-5,5′-diylidene)bis(5-bromo-1-dodecyl-indolin-2-one) (**4b-S1**) and (3*Z*,3′*Z*)-3,3′-((*E*)-1,1,1′,1′-tetraoxido-5*H*,5′*H*-[2,2′-bithiophenyldene]-5,5′-diylidene)bis(6-bromo-1-dodecyl-indolin-2-one) (**4c-S1**), and their use as n-channel semiconductors for organic thin film transistors (OTFTs) are reported. Compared to the non-oxidized parent indophenine compound 3,3′-(5*H*,5′*H*-[2,2′-bithiophenylidene]-5,5′-diylidene)bis(1-dodecylindolin-2-one) (**3a**), **4a-S1** exhibited significantly lower HOMO and LUMO energy levels. Having bromine atoms at the 5,5′- (**4b-S1**) or 6,6′-positions (**4c-S1**), the HOMO and LUMO energy levels further decreased. In OTFT devices, these IDTO compounds exhibit unipolar n-type semiconductor behavior due to their significantly deeper LUMO and HOMO energy levels than those of **3a** that shows ambipolar charge transport performance. The maximum electron mobilities of **4a-S1**, **4b-S1** and **4c-S1** are in the order of 10^{-2} to 10^{-1} cm^2 V^{-1} s^{-1}, which are much higher than that of **3a** ($\sim 10^{-3}$ cm^2 V^{-1} s^{-1}), originating from the lower LUMO energy levels and the high isomeric purities of the former compounds. Among the three IDTO compounds, **4c-S1** shows the highest electron mobility of up to 0.11 cm^2 V^{-1} s^{-1}, which is likely due to its most extended π-electron delocalization on the LUMO wavefunction.

Received 9th March 2016
Accepted 27th April 2016

DOI: 10.1039/c6ra06316k

www.rsc.org/advances

Introduction

In the past few decades, organic thin film transistors (OTFTs) have garnered much attention due to their potential application in flexible and low-cost electronic devices such as radio frequency identification (RFID) tags, smart cards and flexible displays.[1–4] An OTFT device operates in a p-channel (holes as carriers) or n-channel (electrons as carriers) mode, which requires a p-type or n-type organic semiconductor as the channel material, respectively. While a large number of high performance p-type organic semiconductors with mobility comparable to or greater than that of amorphous silicon (Si) have been developed,[5–7] progress of the n-type counterparts has been relatively slow.[8–12]

One key requirement for an n-type organic semiconductor is a low LUMO (the lowest unoccupied molecular orbital) energy level below *ca.* −3.7 to −4.0 eV to facilitate electron injection and stable electron transport.[13–16] Three types of molecular structures have been extensively explored to reach such a low LUMO energy level and to achieve good n-type semiconductor performance, including (1) highly electron-deficient polycyclic rings such as naphthalene diimide (NDI) and perylene diimide (PDI);[17–23] (2) electron-rich building blocks substituted with strong electron-withdrawing groups such as CN- or F-substituted oligothiophenes;[24–28] (3) quinoidal structures such as tetracyanoquinodimethane (TCNQ) and dicyanomethylene-substituted quinoidal oligothiophenes.[15,29–32] Nevertheless, suitable electron accepting building blocks for the construction of n-type organic semiconductors are still limited.

Indophenine, a long-known blue dyestuff discovered in 1879,[33] consists of a planar quinoidal bithiophene structure (Chart 1). Kim *et al.* reported that OTFT devices based on dodecyl-substituted indophenine (R = dodecyl in Chart 1) exhibited ambipolar charge transport characteristics with electron mobility and hole mobility up to 5.0×10^{-3} cm^2 V^{-1} s^{-1} and 3.1×10^{-2} cm^2 V^{-1} s^{-1}, respectively.[34] The LUMO and HOMO (highest occupied molecular orbital) energy levels of this compound are −3.76 eV and −5.25 eV, respectively.[34] To realize unipolar electron transport performance for indophenine derivatives, the HOMO energy level needs to be further deepened to suppress hole injection. Another issue associated with

Department of Chemical Engineering and Waterloo Institute for Nanotechnology (WIN), University of Waterloo, 200 University Ave West, Waterloo, Ontario, N2L 3G1, Canada. E-mail: yuning.li@uwaterloo.ca; Fax: +1 519-888-4347; Tel: +1 519-888-4567 ext. 31105

† Electronic supplementary information (ESI) available. See DOI: 10.1039/c6ra06316k

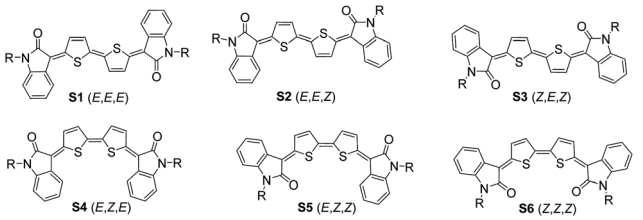

Chart 1 Six possible geometric isomers of indophenine. R = H or alkyl.

indophenine compounds is that they contain six inseparable isomers (Chart 1),[35] making these compounds difficult to self-assemble into highly ordered thin films. To improve the charge carrier mobility of indophenine derivatives, an approach to obtaining a pure isomer form needs to be established. Very recently, we found that dioxidation of the quinoidal bithiophene unit in indophenine could significantly lower the LUMO and HOMO energy levels.[36] Favourably, dioxidation and the subsequent thermally driven isomerization could produce a single isomer product, *i.e.* the (*E*,*E*,*E*)-form thiophene-*S*,*S*-dioxidized indophenine (IDTO). We successfully prepared a copolymer of IDTO and thieno[3,2-*b*]thiophene, which has low LUMO and HOMO energy levels of −3.98 eV and −5.92 eV, respectively, and showed unipolar n-type semiconductor performance in OTFTs.[36]

We found that the IDTO monomer, (3*Z*,3′*Z*)-3,3′-((*E*)-1,1,1′,1′-tetraoxido-5*H*,5′*H*-[2,2′-bithiophenylidene]-5,5′-diylidene) bis(6-bromo-1-(4-octadecyldocosyl)indolin-2-one) (IDTO-40-Br), also has low-lying LUMO (−4.08 eV) and HOMO (−5.91 eV) energy levels, which may be adequate for achieving unipolar n-type semiconductor performance. Small molecule semiconductors are easier to synthesize and have minimal chemical structural defects compared to their polymer counterparts. Unfortunately, IDTO-40-Br has poor crystallinity due to its large 4-octadecyldocosyl (C40) side chains, which were used to solubilize the polymer. In this study, we used shorter and straight dodecyl side chains to improve the crystallinity of IDTO compounds. The effects of bromo-substitution at the 5,5′- or 6,6′-positions of IDTO on the energy levels, crystallinity and charge transport performance were also investigated. These new IDTO compounds showed unipolar n-type semiconductor performance with high electron mobility of up to 0.11 $cm^2 V^{-1} s^{-1}$, which are very promising low-cost solution-processable semiconductors for printed electronics.

Results and discussion

Synthesis and thermal properties

Three isomerically pure IDTO compounds, **4a-S1**, **4b-S1** and **4c-S1**, were synthesized according to the route shown in Scheme 1. Briefly, *N*-dodecyl-substituted isatin compounds **2a**, **2b** and **2c** were synthesized from isatin (**1a**), 5-bromoisatin (**1b**) and 6-bromoisatin (**1c**), respectively. Then **2a**, **2b** and **2c** were reacted with thiophene in toluene at room temperature in the presence of conc. H_2SO_4 to give the alkylated indophenine **3a**, **3b** and **3c**,

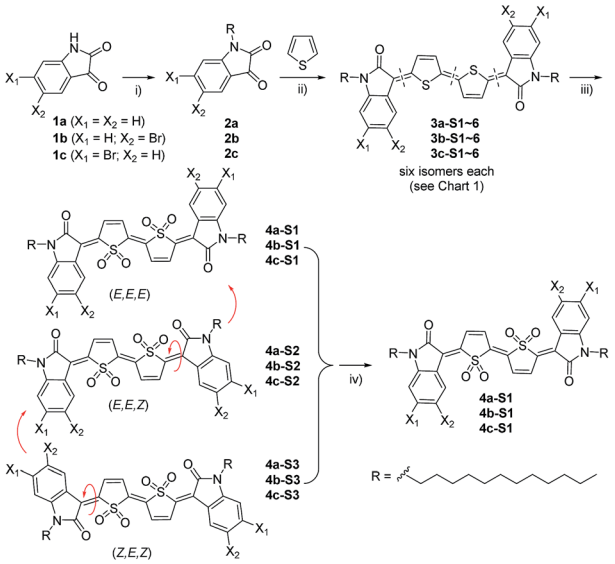

Scheme 1 Synthetic route to thiophene-*S*,*S*-dioxidized indophenine (IDTO) compounds **4a-S1**, **4b-S1** and **4c-S1**. Reagents and conditions: (i) RBr, K_2CO_3, DMF, 70 °C; (ii) thiophene, conc. H_2SO_4, toluene, r.t.; (iii) *m*-CPBA, toluene, r.t.; (iv) toluene, reflux.

respectively. According to the previous studies of indophenine compounds,[34,35] each of these indophenine compounds would contain six inseparable isomers **S1–S6** (Chart 1). The subsequent oxidation was conducted by directly adding 3-chloroperoxybenzoic acid (*m*-CPBA) in one portion to the above reaction mixture at room temperature. We found that this one-pot synthesis is much more convenient and gave better yields of the oxidized products compared to the alternative procedure with (i) purification of **3** by column chromatography and (ii) oxidation with *m*-CPBA. The products from the oxidation step were isolated by a short silica gel column to afford **4a**, **4b** and **4c**, each of which contained three isomers **S1**, **S2** and **S3** (Scheme 1 and Fig. S7†). Then the isomer mixtures were heated in refluxing toluene to convert **S2** and **S3** isomers into the most thermally stable **S1** isomers, **4a-S1**, **4b-S1** and **4c-S1**. The overall yields from **2a**, **2b** and **2c** to **4a-S1**, **4b-S1** and **4c-S1** are 39%, 29% and 49%, respectively.

The thermal stability of **4a-S1**, **4b-S1** and **4c-S1** was evaluated by thermogravimetric analysis (TGA) (Fig. 1). All three compounds showed a two-step degradation process. The first-step weight loss can be ascribed to the elimination of SO_2 due to the relatively labile C–S bonds,[37] while the second-step weight loss was caused by further decomposition of the backbone. The onset decomposition temperatures for **4a-S1**, **4b-S1** and **4c-S1** are 244, 248 and 278 °C, respectively. The much higher decomposition temperature of **4c-S1** than those of **4a-S1** and **4b-S1** might be due to the ability of the 6,6′-dibromo substituents to delocalize π-electrons (see discussions below), making the C–S bonds more stable. We found that the IDTO-based polymer with extended conjugated main chain showed an even higher first onset decomposition temperature of ~335 °C, indicating its more stable C–S bonds.[36] The differential scanning calorimetry (DSC) measurement showed no melting points for all three compounds before decomposition (Fig. S11†).

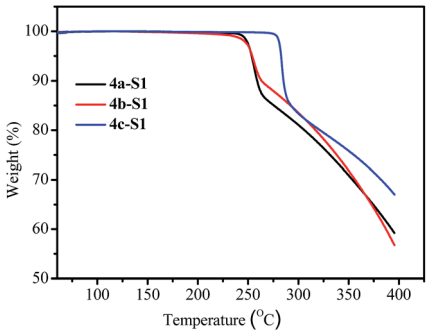

Fig. 1 TGA analysis for **4a-S1**, **4b-S1** and **4c-S1** at a heating rate of 10 °C min^{-1} in N_2 atmosphere.

Theoretical calculations

To gain insight into the electronic properties of **4a-S1**, **4b-S1** and **4c-S1**, molecular geometries and electron distribution of their model compounds (**4a-S1-Me**, **4b-S1-Me** and **4c-S1-Me** in Fig. 2) along with the corresponding (*E*,*E*,*E*)-indophenine compounds (**3a-S1-Me**, **3b-S1-Me** and **3c-S1-Me** in Fig. S8†) were simulated by using density functional theory (DFT). Methyl groups were used in these model compounds to save computation time. The results clearly show that the backbones of these molecules are highly coplanar, indicating that the introduction of the out-of-plane oxygen atoms on the thiophene units have a negligible effect on the backbone planarity. The high coplanarity of the backbone would allow efficient delocalization of the π-electrons and facilitate π–π overlap and intermolecular interaction, thereby enhancing charge transport. The simulation results also indicate that the HOMO and LUMO energy levels of the IDTO compounds are lowered by ~0.75 eV and ~0.35 eV, respectively, compared to their corresponding non-oxidized compounds. It was also found that both HOMO and LUMO energy levels could be further lowered by introducing bromine atoms on the isatin units, which are expected to be more favorable for the electron injection and further inhibit the hole injection, respectively. It should be noted that the 6,6′-dibromo-substituted **4c-S1-Me** has a similar HOMO energy level, but a slightly lower LUMO energy level compared to the 5,5′-dibromo-substituted **4b-S1-Me**. The peripheral bromo substituents on the isatin units can influence the LUMO and HOMO of the molecules through their inductive (electron-withdrawing) and resonance (lone pair electrons) effects. As can be seen in Fig. 2, the 6,6′-dibromo substituents in **4c-S1-Me** participate in both the LUMO and HOMO conjugation paths, largely contributing to the π-electron delocalization in both orbitals by exerting inductive and resonance effects. On the other hand, the 5,5′-dibromo substituents in **4b-S1-Me** participate in the HOMO wavefunction, but not the LUMO wavefunction. The 5,5′-dibromo substituents would exert both inductive and resonance effects on the HOMO energy, but only the inductive effect on the LUMO energy. The different influences of 5- and 6-substitutions of the isatin units on the backbone conjugation were previously found and used to switch the polarity of the carriers of indigo-based polymers between p-type and n-type.[38,39] As a matter of fact, **4b-S1** and **4c-S1** indeed showed quite different charge transport performance, which can be correlated to their different bromo-substitution patterns (to be discussed below).

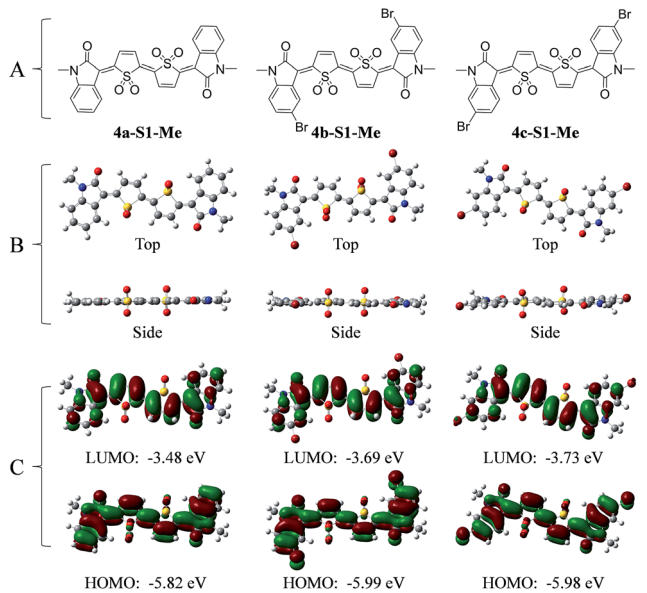

Fig. 2 Chemical structures (A) and the DFT calculation results: optimized molecular geometries (B) and electron density distributions (C) for the IDTO model compounds **4a-S1-Me**, **4b-S1-Me** and **4c-S1-Me**.

Photophysical and electrochemical properties

The photophysical properties of **4a-S1**, **4b-S1** and **4c-S1** were characterized using UV-Vis spectroscopy (Fig. 3 and Table 1). In dilute solutions, all compounds show one major peak and two minor vibronic peaks/shoulders. The λ_{max} red-shifts slightly from 453 nm for **4a-S1** to 456 nm for **4b-S1** and 460 nm for **4c-S1**. The shoulder at ~535 nm for **4c-S1** is much more intense than those of **4a-S1** and **4b-S1**. Going from solution to the solid state, the λ_{max}'s for **4a-S1**, **4b-S1** and **4c-S1** red-shift to 466 nm, 472 nm and 480 nm, respectively, while the long wavelength shoulders also red-shift and become stronger. The E_g^{opt} estimated from the onset wavelengths of the film absorption spectra are 1.74 eV for **4a-S1**, 1.67 eV for **4b-S1** and 1.72 eV for **4c-S1**. Based on the thin film CV diagrams (Fig. 4), the HOMO and LUMO energy levels of **4a-S1** are calculated to be −5.85 eV and −3.99 eV, respectively, while those of **4b-S1** with bromine atoms at the 5,5′-positions

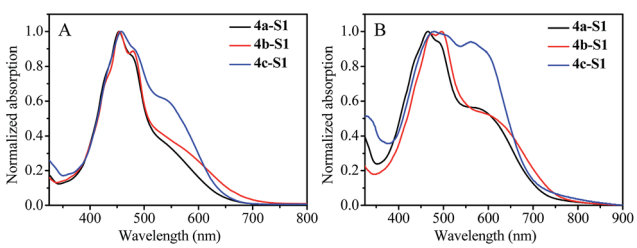

Fig. 3 Normalized absorption spectra of **4a-S1**, **4b-S1** and **4c-S1**: (A) dilute solutions in chloroform; (B) films prepared by spin-coating their chloroform solutions on quartz substrates.

Table 1 Photophysical and electrochemical properties of **4a-S1**, **4b-S1**, and **4c-S1**

	λ_{max} (nm)					
Compound	Solution	Film	E_g^{opt} (eV)	HOMO (eV)	LUMO (eV)	E_g^{CV}[a] (eV)
4a-S1	453, 476 (s),[b] 532 (s)	466, 491 (s), 577 (s)	1.74	−5.85	−3.99	1.86
4b-S1	456, 479 (s), 535 (s)	472, 497 (s), 583 (s)	1.67	−6.33	−4.12	2.21
4c-S1	460, 482 (s), 540 (s)	480, 507 (s), 566 (s)	1.72	−6.30	−4.18	2.12

[a] E_g^{CV} = (LUMO − HOMO) eV. [b] Shoulder.

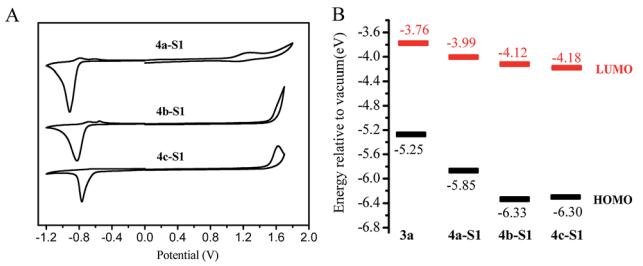

Fig. 4 Cyclic voltammograms (CV) (A) of **4a-S1**, **4b-S1** and **4c-S1** films and energy level diagrams (B) of **3a**,[36] **4a-S1**, **4b-S1** and **4c-S1**, the CV were measured in dry acetonitrile containing 0.1 M n-Bu_4NPF_6 as an electrolyte under nitrogen at a scan rate of 50 mV s^{-1}.

decrease to −6.33 and −4.12 eV, respectively. **4c-S1** with 6,6′-dibromo substituents has a slightly higher HOMO energy level (−6.30 eV) than that of **4b-S1**, which is still much lower than that of **4a-S1**. **4c-S1** has the deepest LUMO energy level of −4.18 eV among three IDTO compounds. These electrochemical data are in good agreement with the DFT calculation results.

Compared to the non-oxidized indophenine **3a**, which showed ambipolar transport performance,[34] the HOMO and LUMO energy levels of **4a-S1**, **4b-S1** and **4c-S1** are significantly deepened, which are beneficial for unipolar electron transport.

Molecular ordering of thin films

Thin films of **4a-S1**, **4b-S1** and **4c-S1** were characterized by using reflection XRD to elucidate their molecular packing features. The thin films were prepared by spin-coating solutions of these compounds onto the dodecyltrichlorosilane (DDTS) modified Si/SiO_2 substrates, optionally followed by annealing at different temperatures. The non-annealed thin films of **4a-S1** and **4b-S1** show intense (100) primary peaks at 7.3° and 5.6°, which correspond to the interlayer lamellar d-spacings of 12.1 Å and 15.78 Å, respectively (Fig. 5). The diffraction peak of **4b-S1** with 5,5′-dibromo substituents is significantly stronger and sharper compared to **4a-S1**, implying the much more ordered molecular packing of the former. Unexpectedly, **4c-S1** with 6,6′-dibromo substituents exhibits a very weak primary peak at 6.5° (d-spacing = 13.6 Å), indicating its poorest crystallinity among the three compounds. These XRD results demonstrate that substitution of the isatin units with bromine atoms and the substitution positions markedly influence the molecular ordering of these compounds. After annealing at 100 °C, the primary peaks of all three compounds intensified significantly. A weak hump appeared at 14.9° for **4a-S1**, which is assigned to the secondary (200) reflection peak, manifesting that higher order crystalline structures formed with the aid of thermal annealing. Interestingly, the primary peak of **4c-S1** shifted from 6.5° to 3.5° (d-spacing = 25.2 Å). Although the molecular packing motif remains as a lamellar structure, the interlayer distance of **4c-S1** increased dramatically (almost doubled), which is also much larger than those of the other two compounds. The reason for such a dramatic change in the crystalline structure of this compound at this temperature is still unclear. Upon annealing at a higher temperature of 150 °C, all films showed further enhanced crystallinity. Since the reflection XRD diagrams of these crystalline thin films only showed the peaks representing the interlayer d-spacings, the molecules of **4a-S1**, **4b-S1** and **4c-S1** presumably adopted an edge-on orientation respective to the substrates. This is beneficial for charge transport through the efficient intermolecular charge hopping along π–π stacks in OTFT devices.

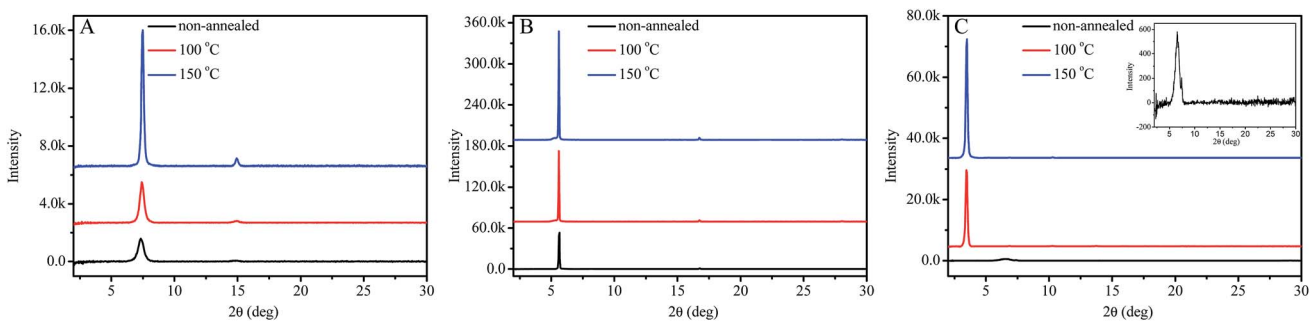

Fig. 5 Out of plane XRD patterns of the thin films on DDTS-modified SiO_2/Si substrate at annealed different temperatures: (A) **4a-S1**; (B) **4b-S1**; (C) **4c-S1**. Inset of (C) enlarged XRD diagram of the non-annealed **4c-S1** thin film.

OTFT performance

To evaluate the charge transport properties of **4a-S1**, **4b-S1** and **4c-S1**, bottom gate bottom contact (BGBC) OTFTs were fabricated using Si wafer having a 300 nm thick insulating SiO_2 layer as the substrate. Au source and drain electrodes were patterned on the substrate by conventional photolithography and thermal deposition techniques. The Si/SiO_2 surface was modified with DDTS to reduce surface charge trapping. The channel semiconductor thin films were spin-coated using 20 mg mL^{-1} chloroform solutions of **4a-S1**, **4b-S1** and **4c-S1** at a spin speed of 5000 rpm for 60 s and then optionally annealed at different temperatures. All devices were fabricated and tested in a nitrogen-filled glove box at room temperature. As shown in Fig. 6, all three compounds displayed unipolar n-type semiconductor characteristics in OTFTs. Table 2 summarized the performance data of the devices. The maximum electron mobilities for these IDTO compounds are in the order of $\sim10^{-2}$ to 10^{-1} cm^2 V^{-1} s^{-1}, which are more than one order of magnitude higher than that of indophenine **3a** ($\sim10^{-3}$ cm^2 V^{-1} s^{-1}).[34] The notable improvements in electron mobility for these IDTO compounds likely originate from (i) their high isomeric purity, which leads to highly ordered molecular packing, and (ii) their much lower LUMO energy levels, which facilitate the electron injection and transport. More importantly, these IDTO compounds showed only n-type semiconductor performance, which is accounted for by their deepened HOMO energy levels that inhibit hole injection and transport.

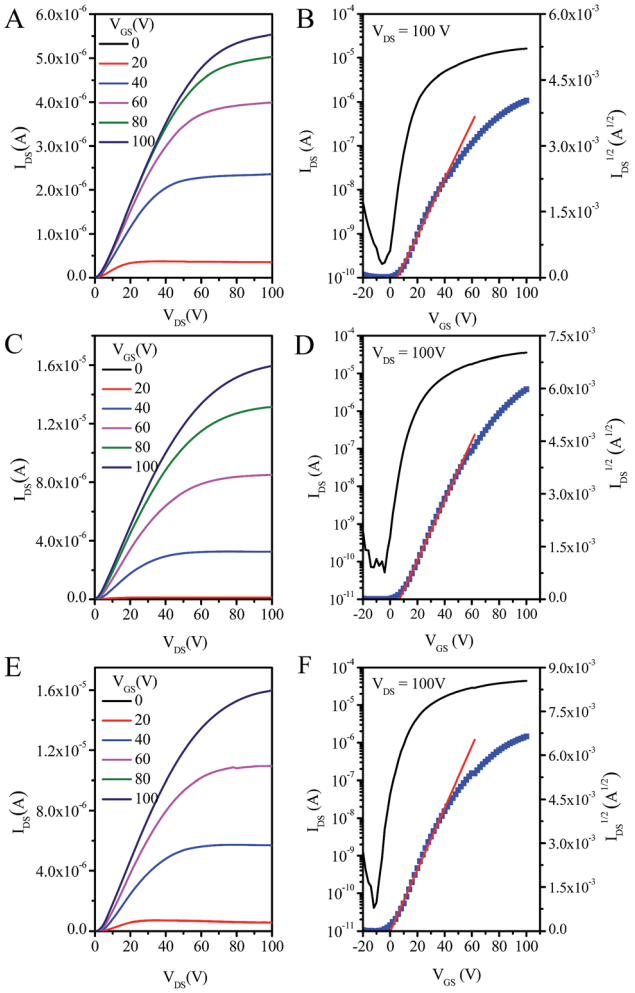

Fig. 6 Output (A, C, and E) and transfer (B, D, and F) characteristics of typical OTFT devices of non-annealed **4a-S1** (A and B), **4b-S1** (C and D) and **4c-S1** (E and F) thin films.

For the non-annealed films, the maximum mobility follows the order of **4c-S1** (0.11 cm^2 V^{-1} s^{-1}) > **4b-S1** (0.071 cm^2 V^{-1} s^{-1}) > **4a-S1** (0.046 cm^2 V^{-1} s^{-1}). Obviously, bromo-substitution is very beneficial for improving electron transport. It is also noted that the 6,6′-dibromo-substituted **4c-S1** showed higher mobility than the 5,5′-dibromo-substituted **4b-S1**. It is known that a higher degree of molecular organization is beneficial for charge transport. The higher crystallinity of the **4b-S1** film might explain its better mobility than that of **4a-S1** (Fig. 5). However, it is not true for the **4c-S1** film because it showed the poorest crystallinity, but exhibited the highest mobility.

As discussed previously, a lower LUMO energy level would reduce the electron injection barrier, which is the difference between the LUMO energy level of the semiconductor and the Fermi energy level of the source electrode (Au was used in this study, which has a Fermi energy level of −4.5 to −5.1 eV (ref. 36 and 40)). The decreasing LUMO energy level order of **4a-S1**, **4b-S1** and **4c-S1**, which are −3.99, −4.12, and −4.18 eV, respectively, appear to follow a trend of increasing mobility. Judging by the regions of their output curves close to the origin in Fig. 6A, C and

Table 2 OTFT device performance of **4a-S1**, **4b-S1**, and **4c-S1**

Compound	Annealing temperature (°C)	μ_{max} (cm^2 V^{-1} s^{-1})	μ_{ave} ± std[b] (cm^2 V^{-1} s^{-1})	V_t[c] (V)	I_{on}/I_{off}[d]
4a-S1	Non-annealed[a]	0.046	0.041 ± 0.0051	5.3 to 7.9	$\sim10^5$
	100	0.030	0.022 ± 0.0059	5.8 to 8.6	$\sim10^4$
	150	0.011	0.008 ± 0.0024	6.3 to 7.4	$\sim10^4$
4b-S1	Non-annealed	0.071	0.055 ± 0.0095	12 to 15	$\sim10^5$
	100	0.053	0.041 ± 0.0900	10 to 14	$\sim10^4$
	150	0.029	0.014 ± 0.0055	12 to 19	$\sim10^4$
4c-S1	Non-annealed	0.110	0.093 ± 0.0027	2.1 to 4.9	$\sim10^5$
	100	0.088	0.069 ± 0.0023	3.8 to 6.2	$\sim10^4$
	150	0.040	0.027 ± 0.0019	2.7 to 5.1	$\sim10^4$

[a] The films were dried briefly at 50 °C to remove the residual solvent. [b] Average mobility obtained from more than four parallel devices at a drain-source voltage of 100 V. [c] Threshold voltage. [d] On–off current ratio.

E, all OTFT devices showed contact resistance, however, the device based on **4c-S1** showed the largest contact resistance. As a result, the greater mobility observed for **4c-S1** compared to that of **4b-S1** cannot be explained by its deeper LUMO energy level.

It has been reported that poor crystallinity and smaller grains of the semiconductor film would form defects and charge traps at the semiconductor/electrode contact interface, leading to an increased contact resistance.[41,42] The lowest degree of crystallinity observed by XRD for the **4c-S1** film substantiates its largest contact resistance. We also examined the morphology of the thin films by atomic force microscopy (AFM) (Fig. 7). The **4c-S1** film showed the smallest grains among the three compounds, which again supports the largest contact resistance observed for the **4c-S1** based OTFT device.

Based on the above discussion, it seems that the differences in crystallinity, LUMO energy levels, and morphology between **4b-S1** and **4c-S1** cannot explain their mobility difference. Therefore, we think that the 6,6′-dibromo substituents in **4c-S1** might have an additional benefit for electron transport compared with the 5,5′-dibromo substituents in **4b-S1**. As observed in the LUMO wavefunctions of their model compounds (Fig. 2), the bromine atoms at the 6,6′-positions in **4c-S1** participate in the backbone conjugation at the LUMO energy level, while the bromine atoms at the 5,5′-positions in **4b-S1** do not. The more extended LUMO π-conjugation path in **4c-S1** would increase the π–π stacking overlap area for more efficient intermolecular electron hopping.

It should be noted that the $I_{DS}^{1/2}$–V_{GS} curves of the OTFT devices of all three compounds are non-linear with steeper slopes in the low V_{GS} regions and shallower slopes in the high V_{DS} regions. This phenomenon has been reported for a number of small molecule and polymer semiconductors in bottom-gated OTFT devices with SAM modified SiO_2 gate dielectric and extensively discussed in several papers.[43–45] It has been accounted for by several possible reasons such as the lower degree of disorder in the bulk than at the semiconductor/contact interface, contact resistance effects, charge trapping in the dielectric layer or interface at higher gate field, the coulombic interactions between the charges at higher gate field, *etc.* As aforementioned, the output curves of the OTFT devices based on these three semiconductors showed contact resistance. In addition, the transfer curves of the OTFT devices based on non-annealed **4a-S1**, **4b-S1** and **4c-S1** thin films with forward and reverse sweep gate voltages were recorded (Fig. S9†). The differences between the forward and reverse sweep transfer curves indicate the hysteresis of the device, which is likely due to the charge trapping.[46] Hence, the non-linearity of the $I_{DS}^{1/2}$–V_{GS} curves observed for these three semiconductors might involve the contact resistance and charge trapping effects.

The mobility values against the gate bias (V_{GS}) for three representative OTFT devices based on **4a-S1**, **4b-S1**, and **4c-S1** (same devices shown in Fig. 6) were plotted and shown in Fig. S10.† When the V_{GS} is < ~30 V, the mobility values followed the order of **4c-S1** > **4b-S1** > **4a-S1**, while when the V_{GS} is > 40 V, the mobility order changed to **4b-S1** > **4c-S1** > **4a-S1**. Their mobility differences become small as V_G increases. The mobility values listed in Table 2 were obtained from the linear fitting of the $I_{DS}^{1/2}$–V_{GS} curves in the low V_{GS} region (V_{GS} < 30 V), which is considered to reflect a more meaningful charge transport parameter.[44]

Post-deposition thermal annealing is widely used to improve the crystallinity of the thin films and thereby their charge carrier mobility. However, we observed that the maximum mobility for the 100 °C-annealed films dropped to 0.030 $cm^2 V^{-1} s^{-1}$ for **4a-S1**, 0.053 $cm^2 V^{-1} s^{-1}$ for **4b-S1** and 0.088 $cm^2 V^{-1} s^{-1}$ for **4c-S1**. When the annealing temperature was increased to 150 °C, the maximum mobilities of **4a-S1**, **4b-S1** and **4c-S1** further decreased to 0.011, 0.029 and 0.040 $cm^2 V^{-1} s^{-1}$, respectively. The drop in mobility with increasing annealing temperature was unexpected because the crystallinity of these annealed films was significantly improved (Fig. 5). Thermal decomposition of these compounds at these temperatures is unlikely according to the TGA data (Fig. 1). Instead, the morphological changes of these annealed films might have caused the degradation of their device performance. In particular, the films annealed at 150 °C underwent dramatic changes in morphology. Compared to the non-annealed films, which contain well-connected worm-like grains, all the 150 °C-annealed films are composed of rather isolated disks with large grain boundaries. The poor connectivity and large gaps between grains would hinder the charge hopping between the grains. Although not visible, the interfacial contact between the thin film and the dielectric layer is expected to be worsened for these annealed films, which is another possible reason for the deteriorated charge transport performance.

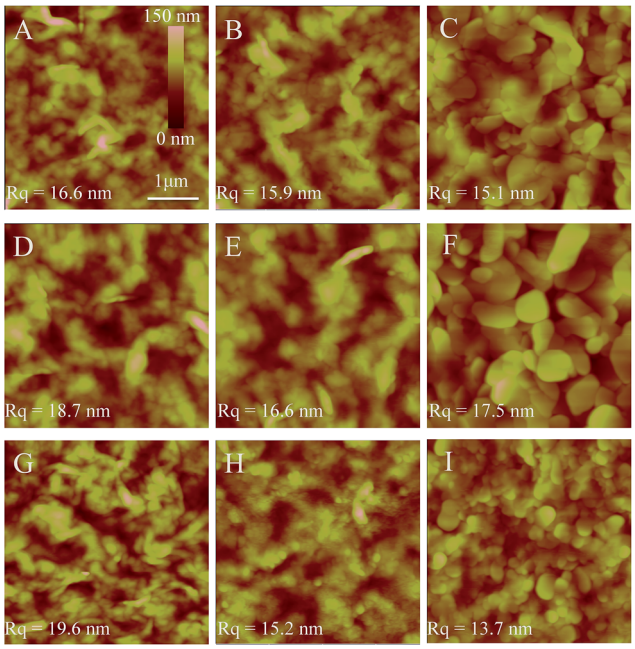

Fig. 7 AFM height images of the films of **4a-S1** (A–C), **4b-S1** (D–F) and **4c-S1** (G–I) at different annealing temperatures: non-annealed (A, D, and G), 100 °C (B, E, and H), and 150 °C (C, F, and I).

Conclusions

Three soluble isomerically pure (*E*,*E*,*E*)-form thiophene-*S*,*S*-dioxidized indophenines, **4a-S1**, **4b-S1** and **4c-S1**, with deep

LUMO energy levels (≤ -3.99 eV) were conveniently synthesized from isatins and thiophene and used as novel n-type organic semiconductors for solution-processed OTFTs. Compared with its non-oxidized parent indophenine compound **3a**, the thiophene-*S*,*S*-dioxidized indophenine compound **4a-S1** has much lower HOMO and LUMO energy levels. Substitution of the 5,5′-postions with bromine atoms could further decrease the HOMO and LUMO energy levels of the resulting **4b-S1** due to their participation in the HOMO path and their inductive effect exerted on the LUMO. 6,6′-Dibromo-substituted **4c-S1** has the lowest LUMO energy level due to the participation of the bromine atoms in both the HOMO and LUMO conjugation paths. **4a-S1** exhibited n-type semiconductor performance in OTFTs with electron mobility up to 0.046 $cm^2\ V^{-1}\ s^{-1}$, which is one order of magnitude higher than that of **3a**. The unipolar electron transport performance and the improved electron mobility are results of the lowered energy levels and the high isomeric purity of **4a-S1**. 5,5′-Dibromo-substituted **4b-S1** showed further improved electron mobility up to 0.071 $cm^2\ V^{-1}\ s^{-1}$ due to its enhanced crystallinity compared to **4a-S1**. The best mobility of 0.11 $cm^2\ V^{-1}\ s^{-1}$ was achieved by **4c-S1**, which is accounted for by its most extended π-conjugation. Our results demonstrated that thiophene-*S*,*S*-dioxidized indophenine compounds are a promising class of novel low-cost n-type semiconductors for printed organic electronics.

Experimental section

Materials and characterization

All starting materials were purchased from commercial sources and used without further purification. NMR data were recorded with a Bruker DPX 300 MHz spectrometer. The chemical shifts of ^{1}H NMR and ^{13}C NMR were referenced to tetramethylsilane (TMS, 0 ppm) and residual $CHCl_3$ in $CDCl_3$, respectively. High resolution mass spectroscopy (HR-MS) data were obtained using Thermo Scientific Q-Exactive Orbitrap. Computational simulations were performed using density function theory (DFT) calculation with the 6-311G+(d,p) basis set and the orbital pictures were obtained using GaussView 5.0 software. Differential scanning calorimetry (DSC) measurements and thermogravimetric analysis (TGA) were carried out on a Perkin-Elmer DSC 7 and a TA Instruments SDT 2960, respectively, at a scan rate of 10 °C min^{-1} under nitrogen. UV-Vis spectra were recorded on a Thermo Scientific Genesys 10 UV instrument using chloroform solutions and films spin-coated onto quartz substrates. Optical band gaps (E_g^{opt}) were calculated from the onset absorption wavelengths (λ_{onset}) of the thin film UV-Vis absorption spectra according to $E_g^{opt} = 1240/\lambda_{onset}$ eV. Cyclic voltammetry (CV) data were obtained on a CHI600E electrochemical analyzer in dry acetonitrile containing 0.1 M *n*-Bu_4NPF_6 as an electrolyte under nitrogen at a scan rate of 50 mV s^{-1}. A three-electrode cell was used, which has platinum wire electrodes as both the counter and working electrode, and Ag/AgCl as the reference electrode. Ferrocene was used as a reference, which has a HOMO energy level of −4.8 eV.[47] HOMO and LUMO levels were calculated using the equations HOMO $= -(4.80 + E_{onset}^{ox})$ eV and LUMO $= -(4.80 + E_{onset}^{re})$ eV, in which E_{onset}^{ox} and E_{onset}^{re} are oxidation and reduction onset potentials in the CV curves, respectively. A Bruker D8 Advance powder Diffractometer with standard Bragg–Brentano geometry was used to collect the XRD patterns of the thin films spin-coated on DDTS-modified Si/SiO_2 substrates using Cu $K_{\alpha 1}$ radiation ($\lambda = 1.5406$ Å), then the same samples were used to record atomic force microscopic (AFM) images with a Dimension 3100 scanning probe microscope.

Fabrication and characterization of OTFT devices

Bottom-contact bottom-gate OTFT devices were fabricated on a heavily n-doped Si/SiO_2 substrate, where the conductive Si layer and the insulating SiO_2 layer function as the gate and dielectric, respectively. The gold source/drain pairs with defined channel length (30 μm) and channel width (1000 μm) were obtained by conventional photolithography and thermal deposition techniques. The Si/SiO_2 substrate was cleaned using ultrasonication in acetone and then isopropanol. Subsequently, the substrates were treated in a solution of DDTS in HPLC grade toluene (10 mg mL^{-1}) at room temperature for 20 min to form a hydrophobic self-assembled monolayer (SAM), followed by washing with HPLC grade toluene to remove the residue DDTS. Then the active layer (~40 nm) was deposited by spin-coating a 20 mg mL^{-1} solution of **4a-S1**, **4b-S1** or **4c-S1** in chloroform at a spin speed of 5000 rpm for 60 s in a glove box. After thermal annealing at a given temperature in the glove box for 20 min, the devices were characterized in the same glove box with an Agilent B2912A Precision Source/Measure Unit. The carrier mobility is calculated in the saturation region according to the following equation:

$$I_D = \frac{W}{2L} C_i \mu (V_G - V_T)^2$$

where I_D is the drain current, W and L are the device channel width and length, C_i is the gate dielectric layer capacitance per unit area (~11.6 nF cm^{-2}), μ is the carrier mobility, V_G is the gate voltage and V_T is the threshold voltage.

Procedure for synthesis

1-Dodecyl-indoline-2,3-dione (2a). To a solution of isatin (**1a**) (1 g, 6.80 mmol) in *N*,*N*′-dimethylformamide (DMF) (20 mL), 1-bromododecane (2.03 g, 8.16 mmol) and K_2CO_3 (1.88 g, 13.59 mmol) were added. The mixture was stirred at 70 °C overnight and then the solvent was removed under reduced pressure. The residue was dissolved in $CHCl_3$ (100 mL) and then washed with water and brine, separated, and dried over $MgSO_4$. After filtration, the solvent was removed *in vacuo* and the crude product was purified by column chromatography on silica gel with hexane/dichloromethane (DCM) with v/v = 1/1 to give **1b** as an orange solid (1.83 g, 86%). ^{1}H-NMR (300 MHz, $CDCl_3$) δ 7.58 (m, 2H), 7.10 (t, $J = 7.5$ Hz, 1H), 6.87 (d, $J = 7.8$ Hz, 1H), 3.70 (t, $J = 7.4$ Hz, 2H), 1.63–1.70 (m, 2H), 1.24–1.33 (m, 18H), 0.87 (t, $J = 5.9$ Hz, 3H).

5-Bromo-1-dodecyl-indoline-2,3-dione (2b). This compound was prepared using 5-bromoisatin (**1b**) following a similar procedure for the preparation of **2a**. Yield: 1.29 g (74%). ^{1}H-

NMR (300 MHz, $CDCl_3$) δ 7.68 (m, 2H), 6.78 (d, $J = 8.8$ Hz, 1H), 3.68 (t, $J = 7.2$ Hz, 2H), 1.65 (m, 2H), 1.23–1.30 (m, 18H), 0.85 (t, $J = 6.2$ Hz, 3H).

6-Bromo-1-dodecyl-indoline-2,3-dione (2c). This compound was prepared using 6-bromoisatin (**1c**) following a similar procedure for the preparation of **2a**. Yield: 1.41 g (81%). ^{1}H-NMR (300 MHz, $CDCl_3$) δ 7.45 (d, $J = 7.9$ Hz, 1H), 7.25 (d, $J = 7.8$ Hz, 1H), 7.04 (s, 1H), 3.67 (t, $J = 7.3$ Hz, 2H), 1.67 (m, 2H), 1.24–1.32 (m, 18H), 0.86 (t, $J = 6.0$ Hz, 3H).

(3*Z*,3′*Z*)-3,3′-((*E*)-1,1,1′,1′-Tetraoxido-5*H*,5′*H*-[2,2′-bithiophenylidene]-5,5′-diylidene)bis(1-dodecyl-indolin-2-one) (4a-S1). Concentrated sulfuric acid (96%, 0.3 mL) was added dropwise to a rapidly stirred solution of **2a** (0.5 g, 1.59 mmol) and thiophene (0.27 g, 3.17 mmol) in toluene (10 mL) at room temperature. After the reaction mixture was stirred for 3 h at room temperature, 3-chloroperoxybenzoic acid (*m*-CPBA) (2.13 g, 77 wt% pure, 9.51 mmol) was added in one portion and the resulting mixture was stirred overnight. Saturated aqueous K_2CO_3 solution (100 mL) was added, then extracted with DCM and washed with saturated aqueous K_2CO_3 solution and dried over anhydrous $MgSO_4$. The solvent was removed *in vacuo* and the crude product was purified by column chromatography on silica gel with hexane/DCM with v/v = 1/3 to give the isomers mixture product (272 mg). Then this mixture was heated in refluxing toluene overnight under nitrogen to afford **4a-S1** as a dark brown solid (259 mg, 39%). ^{1}H NMR (300 MHz,$CDCl_3$): δ 8.66 (d, $J = 8.3$ Hz, 2H), 8.18 (d, $J = 7.8$ Hz, 2H), 7.56 (d, $J = 8.3$ Hz, 2H), 7.37 (m, 2H), 7.05 (m, 2H), 6.79 (d, $J = 7.8$ Hz, 2H), 3.69 (t, $J = 7.0$ Hz, 4H), 1.66 (m, 4H), 1.24–1.32 (m, 36H), 0.86 (t, $J = 6.5$ Hz, 6H). ^{13}C NMR ($CDCl_3$, 75 MHz, ppm): δ 165.9, 145.2, 139.4, 134.3, 134.4, 130.9, 127.7, 126.3, 124.9, 123.0, 118.3, 108.9, 40.1, 31.8, 29.5, 29.4, 29.3, 29.2, 29.1, 27.3, 26.8, 22.6, 13.9. HR-ESI-MS (M^+) calc. for $C_{48}H_{62}N_2O_6S_2^+$, 827.40; found, 827.40981.

(3*Z*,3′*Z*)-3,3′-((*E*)-1,1,1′,1′-Tetraoxido-5*H*,5′*H*-[2,2′-bithiophenylidene]-5,5′-diylidene)bis(5-bromo-1-dodecyl-indolin-2-one) (4b-S1). This compound was prepared using **2b** following a similar procedure for the preparation of **4a-S1**. Yield: 183 mg (29%). ^{1}H NMR (300 MHz, $CDCl_3$): δ 8.65 (d, $J = 8.3$ Hz, 2H), 8.28 (d, $J = 1.7$ Hz, 2H), 7.62 (d, $J = 8.3$ Hz, 2H), 7.49 (dd, $J_1 = 1.7$ Hz, $J_2 = 8.3$ Hz, 2H), 6.68 (d, $J = 8.3$ Hz, 2H), 3.68 (t, $J = 7.1$ Hz, 4H), 1.64 (m, 4H), 1.23–1.30 (m, 36H), 0.86 (t, $J = 6.5$ Hz, 6H). ^{13}C NMR ($CDCl_3$, 75 MHz, ppm): δ 165.5, 142.2, 140.4, 135.9, 134.1, 130.9, 127.5, 126.3, 123.5, 123.0, 119.8, 110.5, 40.3, 31.8, 29.6, 29.5, 29.4, 29.3, 29.2, 27.2, 26.8, 22.6, 14.0. HR-ESI-MS (M^+) calc. for $C_{48}H_{60}Br_2N_2O_6S_2^+$, 983.23; found, 983.23317.

(3*Z*,3′*Z*)-3,3′-((*E*)-1,1,1′,1′-Tetraoxido-5*H*,5′*H*-[2,2′-bithiophenylidene]-5,5′-diylidene)bis(6-bromo-1-dodecyl-indolin-2-one) (4c-S1). This compound was prepared using **2c** following a similar procedure for the preparation of **4a-S1**. Yield: 310 mg (49%). ^{1}H NMR (300 MHz, $CDCl_3$): δ 8.63 (d, $J = 8.3$ Hz, 2H), 8.02 (d, $J = 8.3$ Hz, 2H), 7.57 (d, $J = 8.3$ Hz, 2H), 7.20 (dd, $J_1 = 1.4$ Hz, $J_2 = 8.3$ Hz, 2H), 6.96 (d, $J = 1.4$ Hz, 2H), 3.68 (t, $J = 7.1$ Hz, 4H), 1.65 (m, 4H), 1.24–1.34 (m, 36H), 0.86 (t, $J = 6.5$ Hz, 6H). ^{13}C NMR ($CDCl_3$, 75 MHz, ppm): δ 165.8, 145.9, 139.7, 134.4, 130.9, 128.4, 128.1, 126.9, 125.9, 123.8, 117.1, 112.4, 40.3, 31.8, 29.4, 29.3, 29.2, 29.1, 29.0, 27.2, 26.8, 22.6, 13.9. HR-ESI-MS (M^+) calc. for $C_{48}H_{60}Br_2N_2O_6S_2^+$, 983.23; found, 983.23467.

Acknowledgements

This work is financially supported by the Natural Sciences and Engineering Research Council of Canada (NSERC) Discovery Grants (#402566-2011).

References

1 C. Wang, H. Dong, W. Hu, Y. Liu and D. Zhu, *Chem. Rev.*, 2012, **112**, 2208–2267.
2 Y. Li, P. Sonar, L. Murphy and W. Hong, *Energy Environ. Sci.*, 2013, **6**, 1684–1710.
3 J. Mei and Z. Bao, *Chem. Mater.*, 2014, **26**, 604–615.
4 Z. Yi, S. Wang and Y. Liu, *Adv. Mater.*, 2015, **27**, 3589–3606.
5 J. Li, Y. Zhao, H. S. Tan, Y. Guo, C.-A. Di, G. Yu, Y. Liu, M. Lin, S. H. Lim, Y. Zhou, H. Su and B. S. Ong, *Sci. Rep.*, 2012, **2**, 754.
6 I. Kang, H.-J. Yun, D. S. Chung, S.-K. Kwon and Y.-H. Kim, *J. Am. Chem. Soc.*, 2013, **135**, 14896–14899.
7 G. Kim, S.-J. Kang, G. K. Dutta, Y.-K. Han, T. J. Shin, Y.-Y. Noh and C. Yang, *J. Am. Chem. Soc.*, 2014, **136**, 9477–9483.
8 H. Yan, Z. Chen, Y. Zheng, C. Newman, J. R. Quinn, F. Dotz, M. Kastler and A. Facchetti, *Nature*, 2009, **457**, 679–686.
9 Y. Zhao, Y. Guo and Y. Liu, *Adv. Mater.*, 2013, **25**, 5372–5391.
10 T. Lei, J.-H. Dou, X.-Y. Cao, J.-Y. Wang and J. Pei, *Adv. Mater.*, 2013, **25**, 6589–6593.
11 S. G. Hahm, Y. Rho, J. Jung, S. H. Kim, T. Sajoto, F. S. Kim, S. Barlow, C. E. Park, S. A. Jenekhe, S. R. Marder and M. Ree, *Adv. Funct. Mater.*, 2013, **23**, 2060–2071.
12 B. Sun, W. Hong, Z. Yan, H. Aziz and Y. Li, *Adv. Mater.*, 2014, **26**, 2636–2642.
13 J. Zaumseil and H. Sirringhaus, *Chem. Rev.*, 2007, **107**, 1296–1323.
14 Z. Wang, C. Kim, A. Facchetti and T. J. Marks, *J. Am. Chem. Soc.*, 2007, **129**, 13362–13363.
15 Y. Suzuki, E. Miyazaki and K. Takimiya, *J. Am. Chem. Soc.*, 2010, **132**, 10453–10466.
16 Y. Deng, B. Sun, Y. He, J. Quinn, C. Guo and Y. Li, *Chem. Commun.*, 2015, **51**, 13515–13518.
17 H. E. Katz, A. J. Lovinger, J. Johnson, C. Kloc, T. Siegrist, W. Li, Y.-Y. Lin and A. Dodabalapur, *Nature*, 2000, **404**, 478–481.
18 B. A. Jones, M. J. Ahrens, M.-H. Yoon, A. Facchetti, T. J. Marks and M. R. Wasielewski, *Angew. Chem., Int. Ed.*, 2004, **43**, 6363–6366.
19 B. A. Jones, A. Facchetti, M. R. Wasielewski and T. J. Marks, *J. Am. Chem. Soc.*, 2007, **129**, 15259–15278.
20 Y. Wen, Y. Liu, C. Di, Y. Wang, X. Sun, Y. Guo, J. Zheng, W. Wu, S. Ye and G. Yu, *Adv. Mater.*, 2009, **21**, 1631–1635.
21 X. Zhan, A. Facchetti, S. Barlow, T. J. Marks, M. A. Ratner, M. R. Wasielewski and S. R. Marder, *Adv. Mater.*, 2011, **23**, 268–284.
22 H. Li, F. S. Kim, G. Ren, E. C. Hollenbeck, S. Subramaniyan and S. A. Jenekhe, *Angew. Chem., Int. Ed.*, 2013, **52**, 5513–5517.
23 A. J. Tilley, C. Guo, M. B. Miltenburg, T. B. Schon, H. Yan, Y. Li and D. S. Seferos, *Adv. Funct. Mater.*, 2015, **25**, 3321–3329.

24 A. Facchetti, Y. Deng, A. Wang, Y. Koide, H. Sirringhaus, T. J. Marks and R. H. Friend, *Angew. Chem., Int. Ed.*, 2000, **39**, 4547–4551.
25 M.-H. Yoon, S. A. DiBenedetto, A. Facchetti and T. J. Marks, *J. Am. Chem. Soc.*, 2005, **127**, 1348–1349.
26 F. Babudri, G. M. Farinola, F. Naso and R. Ragni, *Chem. Commun.*, 2007, 1003–1022.
27 H. Tian, Y. Deng, F. Pan, L. Huang, D. Yan, Y. Geng and F. Wang, *J. Mater. Chem.*, 2010, **20**, 7998–8004.
28 L. Wang, X. Zhang, H. Tian, Y. Lu, Y. Geng and F. Wang, *Chem. Commun.*, 2013, **49**, 11272–11274.
29 A. R. Brown, D. M. de Leeuw, E. J. Lous and E. E. Havinga, *Synth. Met.*, 1994, **66**, 257–261.
30 T. M. Pappenfus, R. J. Chesterfield, C. D. Frisbie, K. R. Mann, J. Casado, J. D. Raff and L. L. Miller, *J. Am. Chem. Soc.*, 2002, **124**, 4184–4185.
31 S. Handa, E. Miyazaki, K. Takimiya and Y. Kunugi, *J. Am. Chem. Soc.*, 2007, **129**, 11684–11685.
32 Y. Qiao, Y. Guo, C. Yu, F. Zhang, W. Xu, Y. Liu and D. Zhu, *J. Am. Chem. Soc.*, 2012, **134**, 4084–4087.
33 A. Baeyer, *Ber. Dtsch. Chem. Ges.*, 1879, **12**, 1309–1319.
34 H. Hwang, D. Khim, J.-M. Yun, E. Jung, S.-Y. Jang, Y. H. Jang, Y.-Y. Noh and D.-Y. Kim, *Adv. Funct. Mater.*, 2015, 1146–1156.
35 G. V Tormos, K. A. Belmore and M. P. Cava, *J. Am. Chem. Soc.*, 1993, **115**, 11512–11515.
36 Y. Deng, B. Sun, Y. He, J. Quinn, C. Guo and Y. Li, *Angew. Chem., Int. Ed.*, 2016, **55**, 3459–3462.
37 E. Amir, K. Sivanandan, J. E. Cochran, J. J. Cowart, S.-Y. Ku, J. H. Seo, M. L. Chabinyc and C. J. Hawker, *J. Polym. Sci., Part A: Polym. Chem.*, 2011, **49**, 1933–1941.
38 C. Guo, J. Quinn, B. Sun and Y. Li, *J. Mater. Chem. C*, 2015, **3**, 5226–5232.
39 C. Guo, J. Quinn, B. Sun and Y. Li, *Polym. Chem.*, 2015, **6**, 6998–7004.
40 A. Wan, J. Hwang, F. Amy and A. Kahn, *Org. Electron.*, 2005, **6**, 47–54.
41 W.-K. Kim and J.-L. Lee, *Appl. Phys. Lett.*, 2006, **88**, 262102.
42 S. Yadav, P. Kumar and S. Ghosh, *Appl. Phys. Lett.*, 2012, **101**, 193307.
43 D. Braga and G. Horowitz, *Adv. Mater.*, 2009, **21**, 1473–1486.
44 H. Sirringhaus, *Adv. Mater.*, 2014, **26**, 1319–1335.
45 E. G. Bittle, J. I. Basham, T. N. Jackson, O. D. Jurchescu and D. J. Gundlach, *Nat. Commun.*, 2016, **7**, 10908.
46 H. Sirringhaus, *Adv. Mater.*, 2014, **26**, 1319–1335.
47 B. W. D'Andrade, S. Datta, S. R. Forrest, P. Djurovich, E. Polikarpov and M. E. Thompson, *Org. Electron.*, 2005, **6**, 11–20.